Permeability and conductivity for reconstruction models of porous media

R. Hilfer[1,2] and C. Manwart[1]
[1]*ICA-1, Universität Stuttgart, Pfaffenwaldring 27, 70569 Stuttgart, Germany*
[2]*Institut für Physik, Universität Mainz, 55099 Mainz, Germany*
(Received 27 October 2000; published 26 July 2001)

The purpose of this paper is to examine representative examples of realistic three-dimensional models for porous media by comparing their geometrical and transport properties with those of the original experimental specimen. The comparison is based on numerically exact evaluations of permeability, formation factor, porosity, specific internal surface, mean curvature, Euler number, local porosity distributions, and local percolation probabilities. The experimental specimen is a three-dimensional computer tomographic image of Fontainebleau sandstone. The three models are examples of physical and stochastic reconstructions for which many of the geometrical characteristics coincide with those of the experimental specimen. We find that in spite of the similarity in the geometrical properties the permeability and formation factor can differ greatly between models and experiment. Our results seem to indicate that the truncation of correlations is responsible for some of these observed discrepancies. A physical reconstruction model by Bakke and Øren [SPEJ **2**, 136 (1997)] based on sedimentation, compaction and diagenesis of sandstones yields surprisingly accurate predictions for permeability and conductivity. These findings imply that many of the presently used geometric descriptors of porous media are insufficient for the prediction of transport.

DOI: 10.1103/PhysRevE.64.021304 PACS number(s): 81.05.Rm, 61.43.Gt, 83.85.Pt

A great deal of research activity in physics has recently been focussed on transport in porous media [1–7] because the theory of porous media underlies many unsolved problems in the applied and engineering sciences ranging from geophysics [8] and petroleum engineering [6] to contaminant transport [9] and paper manufacturing [10]. Despite many years of research there is still no agreement on the basic question of which macroscopic geometrical observables besides porosity are needed to predict macroscopic transport parameters such as hydraulic permeability or electrical conductivity of a given porous microstructure [2,11].

Most works on transport through porous media assert the validity of a specific model for the porous microstructure and proceed by calculating physical properties for the model rather than for the original microstructure itself [12–14,6]. A multitude of porous media models has been proposed that may be roughly divided into reconstruction models, that attempt to reconstruct a realistic three-dimensional pore structure [15], and nonreconstruction models, such as the classical capillary tube model [16] or network models [12,17], that postulate an artificial model geometry. In this paper our objective is to compare exact geometrical and transport properties of three realistic three-dimensional models for Fontainebleau sandstone with those of an experimental specimen. One of our motivations has been to test the reliability of two so-called reconstruction models that have recently found much attention [18,19]. Reconstruction models are models that attempt to reconstruct the experimental porous microstructure usually in a statistical sense. Equally important has been our second motivation, namely, to find reliable correlations between the geometric characteristics of a porous microstructure and its transport properties. Most important for practical purposes would be the identification of geometrical observables that allow to predict permeability and electrical conductivity.

Direct comparisons between different reconstruction models have, to the best of our knowledge, not been carried out in the literature. Establishing direct comparisons between different models is needed not only for academic research purposes but also for applications in hydrology or petroleum engineering. In this paper we start the systematic comparison of models for the popular and well studied example of Fontainebleau sandstone.

Given a porous sample $\mathbb{S}\subset\mathbb{R}^3$, such as a piece of Fontainebleau sandstone, with pore space $\mathbb{P}$ and matrix space $\mathbb{M}$ with $\mathbb{P}\cup\mathbb{M}=\mathbb{S}$ and $\mathbb{P}\cap\mathbb{M}=\varnothing$ we assume that the internal boundaries (i.e., the difference between the closure and the interior) coincide, i.e., $\partial\mathbb{P}=\partial\mathbb{M}$. Let the porous sample $\mathbb{S}$ have the shape of a cube or rectangular parallelepiped with sidelengths L_i $(i=x,y,z)$, and let it be discretized into cubic voxels of side length a such that $L_i=M_i a$. On the microscopic (pore) scale the boundary value problem for stationary creeping fluid flow of an incompressible Newtonian fluid reads

$$\eta\Delta\mathbf{v}(\mathbf{r})-\nabla p(\mathbf{r})=\mathbf{0},\quad \mathbf{r}\in\mathbb{P} \tag{1a}$$

$$\nabla\cdot\mathbf{v}(\mathbf{r})=\mathbf{0},\quad \mathbf{r}\in\mathbb{P} \tag{1b}$$

$$\mathbf{v}(\mathbf{r})=\mathbf{0},\quad \mathbf{r}\in\partial\mathbb{P} \tag{1c}$$

where $\mathbf{v}(\mathbf{r})$ and $p(\mathbf{r})$ denote the microscopic velocity and pressure fields that may be extended to all of $\mathbb{S}$ by setting them to zero on $\mathbb{M}$. Recalling electrodynamics in the quasistatic approximation the equations of motion for electrical conduction at zero frequency become

$$\mathbf{j}(\mathbf{r})+\sigma(\mathbf{r})\nabla U(\mathbf{r})=\mathbf{0},\quad \mathbf{r}\in\mathbb{S} \tag{2a}$$

$$\nabla\cdot\mathbf{j}(\mathbf{r})=0,\quad \mathbf{r}\in\mathbb{S} \tag{2b}$$

$$\lim_{\mathbf{x}\to\mathbf{r}} \mathbf{n}(\mathbf{r})\cdot\mathbf{j}(\mathbf{x})[\chi_{\mathbb{P}}(\mathbf{x})-\chi_{\mathbb{M}}(\mathbf{x})]=0, \quad \mathbf{r}\in\partial\mathbb{P} \tag{2c}$$

$$\lim_{\mathbf{x}\to\mathbf{r}} \mathbf{n}(\mathbf{r})\times\nabla U(\mathbf{x})[\chi_{\mathbb{P}}(\mathbf{x})-\chi_{\mathbb{M}}(\mathbf{x})]=\mathbf{0}, \quad \mathbf{r}\in\partial\mathbb{P} \tag{2d}$$

where $\mathbf{j}$ is the electrical current density, U is the electrical potential, and the electrical conductivity $\sigma(\mathbf{r})$ is position dependent according to $\sigma(\mathbf{r})=\sigma_{\mathbb{P}}\chi_{\mathbb{P}}(\mathbf{r})+\sigma_{\mathbb{M}}\chi_{\mathbb{M}}(\mathbf{r})$ with $\sigma_{\mathbb{P}},\sigma_{\mathbb{M}}$ being the conductivities of the pore space and matrix space, and $\chi_{\mathbb{P}},\chi_{\mathbb{M}}$ the indicator functions of pore and matrix space $[\chi_{\mathbb{G}}(x)=1$ for $x\in\mathbb{G},\chi_{\mathbb{G}}(x)=0$ for $x\notin\mathbb{G}]$. In the special case of zero matrix conductivity, $\sigma_{\mathbb{M}}=0$, the electrical problem reduces to a potential equation that resembles the fluid flow equations. Additional no-flow boundary conditions are imposed on the surfaces of $\mathbb{S}$ parallel to the main flow direction. Most experiments measure averaged quantities such as the macroscopic permeability, and hence we need to describe briefly how these are obtained from our numerical solutions.

The macroscopic permeability is calculated as follows. First the microscopic pressure and velocity fields are obtained by solving the boundary value problem (1) for a pressure gradient applied along the x direction. Let $\overline{p}_{x0}$ denote the inlet pressure, i.e., the pressure applied to the plane $x=0$, and let $\overline{p}_{xL}$ denote the outlet pressure, i.e., the fluid pressure applied at the plane $x=L_x$, where $L_x=M_x a$ denotes the distance between the inlet and the outlet. Then the first row of the permeability tensor is obtained from Darcys law as

$$\mathbf{k}_x=(k_{xx},k_{xy},k_{xz})=\frac{\eta L_x}{\overline{p}_{x0}-\overline{p}_{xL}}\,\overline{\mathbf{v}}, \tag{3}$$

where the averaged velocity is defined as

$$\overline{\mathbf{v}}=\frac{1}{|\mathbb{S}|}\int_{\mathbb{S}}\mathbf{v}(\mathbf{r})d\mathbf{r}, \tag{4}$$

and $|\mathbb{S}|$ denotes the volume of the set $\mathbb{S}$. The second and third row of the permeability tensor are obtained analogoulsy by applying a pressure gradient along the y or z direction. Similarly the macroscopic effective conductivity tensor is calculated by solving the potential problem (2) for an applied potential along the x direction. The first row of the conductivity tensor is given as

$$\sigma_x=(\sigma_{xx},\sigma_{xy},\sigma_{xz})=\frac{L_x}{\overline{U}_{x0}-\overline{U}_{xL}}\,\overline{\mathbf{j}}, \tag{5}$$

where

$$\overline{\mathbf{j}}=-\frac{1}{|\mathbb{S}|}\int_{\mathbb{S}}\nabla U(\mathbf{r})d\mathbf{r}, \tag{6}$$

and $\overline{U}_{x0}$ and $\overline{U}_{xL}$ are the potentials applied to the plane $x=0$ and $x=L_x$, respectively.

TABLE I. Geometric properties of the four porous samples. ϕ is the porosity, S is the specific surface, κ is the mean curvature, and E is the Euler number, all calculated according to the methods in [22]. S_G is the specific surface calculated from the slope of the correlation function.

	EX	DM	SA	SK
ϕ	0.1355	0.1356	0.1354	0.1355
S_G (mm^{-1})	10.4	10.933	11.067	10.42
S (mm^{-1})	9.99	10.3	11.04	10.21
κ (mm^{-2})	−151	−194	−222	−118
E (mm^{-3})	−172	−220	1153	776

We consider the above boundary value problems for four particular porous samples EX, DM, SA, and SK. The sample EX is a fully three-dimensional computer tomographic image of a Fontainebleau sandstone with resolution $a=7.5\,\mu$m and sidelengths $M_x=299$, $M_y=300$, and $M_z=300$. The other three pore spaces are models. The first model $\mathbb{S}_{\mathrm{DM}}$ is a physical reconstruction model where DM stands for ''diagenesis model.'' The model mimicks sedimentation, compaction, and diagenesis of sand grains. It is constructed to match the porosity and grain size distribution of the Fontainebleau sandstone [18]. The second model SA is a stochastic reconstruction model based on simulated annealing techniques [19]. It is constructed to match porosity, specific internal surface and two-point correlation function. The resolution of all models is $a=7.5\,\mu$m. The size of the SA and SK model is $M_x=M_y=M_z=256$, while that of the DM model is $M_x=M_y=M_z=255$.

The model SK, presented here for the first time, combines features from physical and stochastic reconstruction models. Its idea is to use the simulated annealing algorithm but to update only a subset of all voxels. In the present implementation an initial configuration is constructed as follows. First a close packing of hard spheres with diameters uniformly distributed in the range of $13.6a-18.4a$ is produced. The remaining pore space between spheres is then filled randomly with matrix voxels until the desired porosity of $\phi=0.1355$ is obtained. The added matrix voxels in the initial configuration are declared movable, while the original matrix voxels in the spheres are immovable. The movable matrix voxels are updated sequentially in the same manner as in the SA algorithm until a specified set of geometric observables has been matched exactly. Of course, other initial configurations and another separation into movable and immovable voxels are possible. In the present implementation we match the two-point correlation function in 13 different directions. We choose many directions to improve the isotropy of the resulting reconstruction. Simpler implementations with fewer directions were found to be potentially anisotropic [20] depending on the nature of the reconstructed correlation function. For more details of the model we refer to [21].

We collect the basic geometrical properties of the four samples in Table I. The first row is the porosity ϕ, i.e., the volume fraction of pore space. The second row gives the specific internal surface, i.e., the ratio of internal surface area to sample volume, measured from the slope of the correla-

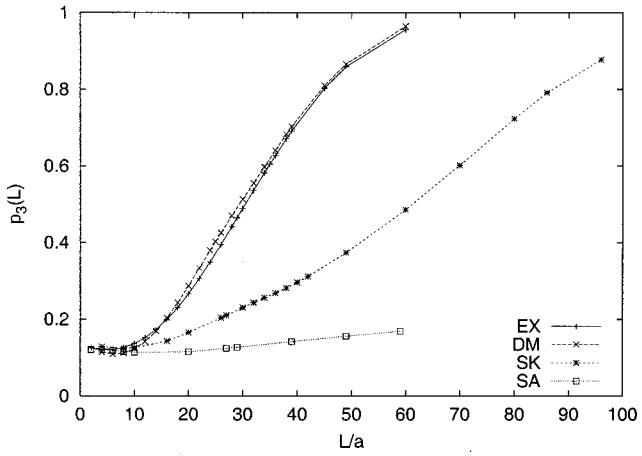

FIG. 1. Total fraction of sub-blocks of sidelength L that are percolating in all three coordinate directions as a function of the sub-blocks' sidelength L. Percolating in the x, y, or z direction means that the sub-block contains a path inside the pore space that connects opposite faces perpendicular to the x, y, or z direction. Each sub-block is analyzed using a Hoshen-Kopelman algorithm.

tion function according to the formula $S_G=-4dS(0)/dr$ where $S(r)$ denotes the voxel-voxel correlation function [2]. The third row is again an estimator for the specific internal surface calculated not from the correlation function but from integral geometric formulas as described in detail in [22]. The third row gives the integral of the mean curvature κ calculated recursively according to Hadwigers theory [22], and the fourth row is the Euler or connectivity number E giving a measure of the number of connectedness components per unit volume. A positive sign of κ indicates that the matrix space is on average convex shaped, while a negative number indicates concavity of $\mathbb{M}$. A positive Euler number E indicates that on average there are isolated components of $\mathbb{M}$ while a negative value indicates the presence of isolated pores. For a detailed description and the geometric characteristics of the samples EX, DM, and SA we refer to [23].

The porosity ϕ and the specific surface S of all four samples are identical within the statistical uncertainties. Of course this follows by definition for the reconstruction models, while in the DM sample it is accidentally true. We also find that the average mean curvature is very similar in all models. We attribute the fact that it is negative to the creases and sharp corners. A clear difference between EX and DM on the one hand and SA, SK on the other appears for the Euler number E. A more detailed geometrical analysis [24,23] based on local porosity theory [2] reveals that the three models DM, SA, and SK are more homogeneous in their geometrical properties than the experimental sample EX. The pore walls of EX and DM are smoother than those of SK and SA. Furthermore we find differences in the connectivity properties. A first indication of this fact can be seen from the value of the specific Euler number E. A clearer view of the phenomenon is obtained using the total fraction of percolating cells introduced in local porosity theory [25]. The total fraction of percolating cells gives the fraction of cubic subblocks of sidelength L that are percolating in all three coordinate directions. A sub-block is called percolating in the x direction if it contains a path inside the pore-space connecting the two opposite faces of the sample that are perpendicular to the x direction (see Fig. 1). In Ref. [23] it was shown that the total fraction of percolating cells is very similar for EX and DM. On the other hand, sample SA was found to have much lower connectivity (see Fig. 13 of [23]). We have evaluated the total fraction of percolating cells also for the SK model and it falls roughly half way between the curves for EX and SA. Based on the clear differences in connectivity seen in these data it was conjectured in [23] that the $p_3(L)$ function from local porosity theory is a geometrical indicator for permeability and conductivity.

TABLE II. Physical transport properties of the four porous samples. σ_{ii} is the conductivity in the direction $i=x,y,z$ in units of $10^{-3}\sigma_{\mathbb{P}}$; k_{ii} is the permeability in mD.

	EX	DM	SA	SK
k_{zz} (mD)	692	923	35	505
k_{yy} (mD)	911	581	22	522
k_{xx} (mD)	790	623	20	497
σ_{zz} $(10^{-3}\sigma_{\mathbb{P}})$	18.5	26.2	1.35	10.4
σ_{yy} $(10^{-3}\sigma_{\mathbb{P}})$	21.9	17.0	0.87	10.2
σ_{xx} $(10^{-3}\sigma_{\mathbb{P}})$	20.5	17.1	0.96	10.1

To test the local percolation probabilities as predictors for transport [23] we have calculated the exact values of permeability and conductivity by solving the above boundary value problems (1) and (2) for all four samples. We have carried out the numerical calculation of the fluid permeability within the complex pore-space geometry. This is a demanding task in terms of computation time and memory. For the above geometries with up to 27×10^6 grid points such calculations of k are possible only on parallel computers. One has to solve simultaneously the steady-state Stokes equation and the condition of incompressibility. We have used an iterative pressure correction algorithm and an artificial compressibility method [26]. On the sample surface the pressure is fixed while von Neumann conditions are applied for the velocity. The iterative algorithm for the solution of Eq. (1) was terminated when the condition $\max_{\mathbf{r}\in\mathbb{P}}|\Delta\mathbf{v}(\mathbf{r})-\nabla p(\mathbf{r})|<10^{-6}$ for the dimensionless left hand side of Eq. (1a) was fulfilled for the first time. Typically the convergence required between 10 000 and 50 000 iterations in the pressure correction equation for samples EX, DM, and SK. The program was run on a CrayT3E with usually 128 processors in parallel, and required between 1 and 3 h run time. For sample SA on the other hand the number of iterations increased by roughly a factor of 10. This was a consequence of the poor connectivity of the sample.

The calculation of the effective conductivity is simpler than the calculation of the fluid permeability because only a Laplace equation for the electrical potential has to be solved. On the matrix-pore interface we apply no-flow boundary conditions, i.e., the matrix phase is insulating $\sigma_{\mathbb{M}}=0$. On the sample surface the potential is fixed while we assume von Neumann conditions for the electric current.

The first three rows of Table II give the numerical results for diagonal elements k_{xx},k_{yy},k_{zz} of the fluid permeability

tensor. The off-diagonal elements were found to be small. Their numerical value was in all cases at least one order of magnitude below the smallest diagonal element, and hence we neglect them here. The permeability of DM is found to be in good agreement with the original sandstone EX. This finding agrees with the coincidence of DM and EX in the total fraction of percolating cells found above, and seen in Fig. 13 of Ref. [23]. Moreover the DM sample is clearly anisotropic having a significantly higher permeability in the *z* direction than in the *x* and *y* directions. This was also predicted by the purely geometrical local porosity analysis in [23]. On the other hand the permeability of the simulated annealing reconstructions SA is an order of magnitude smaller. Thus the stochastic models fail in reconstructing the high degree of geometrical connectivity of the original sandstone, which is an indispensable precondition for high dynamical connectivity. The truncation of correlations in the stochastic models destroys the connectivity that is a long range correlated property. The connectivity correlation length of SA seems to be of the order of the system size. We thus expect that the truncation of correlations will render the SA model nonpercolating at larger system sizes. We can, however, at present not ascertain this expectation because of limited computing resources.

The hybrid model SK gives results intermediate between those for SA and DM. The transport parameters agree better than those of SA, but there is still a significant difference with the results from DM. The intermediate degree of connnectivity is also reflected in the total fraction of percolating cells as discussed above. When plotted in Fig. 13 of Ref. [23] it falls half way between the curves for EXand SA. The results indicate that the geometric quantities of local porosity theory seem to correlate well with transport parameters.

In the fourth, fifth, and sixth row of Table II we present the numerical results for the diagonal components of the conductivity tensor. Again, the values for EX and DM are close to each other. Sample DM exhibits clear anisotropy while the results for SA are again an order of magnitude smaller. We observe the same dependence of the computation time on the geometry as in the case of the fluid permeability. Thus the conductivity results corroborate those for the permeability.

We conclude the discussion by summarizing two consequences of the results found in this work. First we find that stochastic reconstruction models for the two-point correlation function tend to truncate the higher order correlations that exist in natural pore spaces. These correlations are expected to be crucial for the connectivity of the medium and hence for its transport properties [2,11]. Second we note that the geometrical concept of local percolation probabilities introduced in local percolation theory [25] seems to be a useful geometrical observable that correlates with physical observables determining transport.

We thank J. Widjajakusuma, Dr. B. Biswal, Dr. S. Bakke, Dr. P.E. Øren, and Dr. S. Torquato for many discussions and collaboration. We are grateful to the Deutsche Forschungsgemeinschaft for financial support.

[1] M. Sahimi, *Flow and Transport in Porous Media and Fractured Rock* (VCH Verlagsgesellschaft mbH, Weinheim, 1995).
[2] R. Hilfer, Adv. Chem. Phys. **XCII**, 299 (1996).
[3] H. Makse *et al.*, Phys. Rev. E **54**, 3129 (1996).
[4] A. Koponen *et al.*, Phys. Rev. Lett. **80**, 716 (1998).
[5] J. Andrade *et al.*, Phys. Rev. Lett. **79**, 3901 (1997).
[6] P. King *et al.*, Physica A **274**, 60 (1999).
[7] C. van Siclen, Phys. Rev. E **59**, 2804 (1999).
[8] P. Doyen, J. Geophys. Res. **93**, 7729 (1988).
[9] R. Helmig, *Multiphase Flow and Transport Processes in the Subsurface* (Springer, Berlin, 1997).
[10] A. Koponen, M. Kataja, and J. Timonen, Phys. Rev. E **54**, 406 (1996).
[11] R. Hilfer, in *Räumliche Statistik und Statistische Physik*, edited by D. Stoyan and K. Mecke (Springer, Berlin, 2000), p. 203.
[12] I. Fatt, AIME Pet. Trans. **207**, 144 (1956).
[13] M. Dias and A. Payatakes, J. Fluid Mech. **164**, 305 (1986).
[14] M. Blunt and P. King, Phys. Rev. A **42**, 4780 (1990).
[15] P. Adler, *Porous Media* (Butterworth-Heinemann, Boston, 1992).
[16] A. Scheidegger, *The Physics of Flow Through Porous Media* (University of Toronto Press, Toronto, 1974).
[17] A. Payatakes, C. Tien, and R. Turian, AIChE J. **19**, 58 (1973).
[18] S. Bakke and P. Øren, SPE J **2**, 136 (1997).
[19] C. Yeong and S. Torquato, Phys. Rev. E **57**, 495 (1998).
[20] C. Manwart and R. Hilfer, Phys. Rev. E **59**, 5596 (1999).
[21] C. Manwart, Ph.D. thesis, Universität Stuttgart, 2000.
[22] C. Lang, J. Ohser, and R. Hilfer, J. Micros. (to be published).
[23] B. Biswal *et al.*, Physica A **273**, 452 (1999).
[24] B. Biswal, C. Manwart, and R. Hilfer, Physica A **255**, 221 (1998).
[25] R. Hilfer, Phys. Rev. B **44**, 60 (1991).
[26] R. Peyret and T. Taylor, *Computational Methods for Fluid Flow* (Springer-Verlag, Berlin, 1983).